AD A125399

PSR Report 1210

ANALYSIS OF THE LARGE URBAN FIRE ENVIRONMENT

Part I. Theory

By
D. A. Larson
R. D. Small

July 1982

Final Report
Contract EMW-C-0747, Work Unit 2564E

For
Federal Emergency Management Agency
National Preparedness Programs
Washington, D.C. 20472

Approved for Public Release: Distribution Unlimited

PACIFIC-SIERRA RESEARCH CORP.
12340 Santa Monica Blvd. • Los Angeles, CA 90025 • (213) 820-2200

PSR Report 1210

ANALYSIS OF THE LARGE URBAN FIRE ENVIRONMENT

Part I. Theory

By
D. A. Larson
R. D. Small

July 1982

Final Report
Contract EMW-C-0747, Work Unit 2564E

For
Federal Emergency Management Agency
National Preparedness Programs
Washington, D.C. 20472

FEMA Review Notice

This report has been reviewed in the Federal Emergency Managment Agency and approved for publication. Approval does not signify that the contents necessarily reflect the views and policies of the Federal Emergency Management Agency.

Approved for Public Release: Distribution Unlimited

PACIFIC-SIERRA RESEARCH CORP.
12340 Santa Monica Blvd. • Los Angeles, CA 90025 • (213) 820-2200

SECURITY CLASSIFICATION OF THIS PAGE (When Data Entered)

REPORT DOCUMENTATION PAGE		READ INSTRUCTIONS BEFORE COMPLETING FORM
1. REPORT NUMBER PSR Report 1210	2. GOVT ACCESSION NO. AD-A125 399	3. RECIPIENT'S CATALOG NUMBER
4. TITLE (and Subtitle) ANALYSIS OF THE LARGE URBAN FIRE ENVIRONMENT PART I. THEORY		5. TYPE OF REPORT & PERIOD COVERED Final Report September 1981 - September 1982
		6. PERFORMING ORG. REPORT NUMBER PSR Report 1210
7. AUTHOR(s) D. A. Larson, R. D. Small		8. CONTRACT OR GRANT NUMBER(s) EMW-C-0747
9. PERFORMING ORGANIZATION NAME AND ADDRESS Pacific-Sierra Research Corporation 12340 Santa Monica Boulevard Los Angeles, California 90025		10. PROGRAM ELEMENT, PROJECT, TASK AREA & WORK UNIT NUMBERS Work Unit 2564E
11. CONTROLLING OFFICE NAME AND ADDRESS Federal Emergency Management Agency National Preparedness Programs Washington, D.C. 20472		12. REPORT DATE July 1982
		13. NUMBER OF PAGES 34
14. MONITORING AGENCY NAME & ADDRESS(if different from Controlling Office)		15. SECURITY CLASS. (of this report) Unclassified
		15a. DECLASSIFICATION DOWNGRADING SCHEDULE

16. DISTRIBUTION STATEMENT (of this Report)

Approved for public release: distribution unlimited.

17. DISTRIBUTION STATEMENT (of the abstract entered in Block 20, if different from Report)

18. SUPPLEMENTARY NOTES

19. KEY WORDS (Continue on reverse side if necessary and identify by block number)

Fire	Nuclear effects
Large area fire	Fire model
Mass fire	Combustion zone
Firestorm	Urban fire

20. ABSTRACT (Continue on reverse side if necessary and identify by block number)

The strongly buoyant flow generated in and around a large area fire is analyzed. Jump conditions applicable at the fire periphery are used to effect model problem closure, thus permitting calculations of induced fire winds independent of a far-field analysis. Combustion processes are modeled by a volume heat addition. The induced flow is compressible, with arbitrary changes in temperature and density allowed. In one parameter limit, the model equations can be solved exactly. The resulting solution concisely describes the basic

DD FORM 1 JAN 73 1473 EDITION OF 1 NOV 65 IS OBSOLETE

SECURITY CLASSIFICATION OF THIS PAGE (When Data Entered)

20. (cont.)

interchanges of energy and momentum as well as the role of pressure gradients in fire-wind generation. In general, the localized analysis provides a framework for detailed studies of the complex physics of fire-generated flows without recourse to extensive numerical computations involving the far field.

The analysis is applied in simulations of the "turning region" environment created by (1) an experimental, multiple-fuel-bed Flambeau fire, and (2) the World War II Hamburg firestorm. Computed results duplicate observed flow patterns and are consistent with reported data.

PREFACE

This report is the first of the two-part final documentation of Pacific-Sierra Research Corporation's analysis of the large urban fire environment. This part develops the theory underlying the analysis. Parameter studies and simulations of model urban areas are presented in the second part. All work was performed for the Federal Emergency Management Agency under contract EMW-C-0747; the technical monitor was Dr. David Bensen.

The authors gratefully acknowledge the many valuable suggestions of Dr. Harold L. Brode.

SUMMARY

This report analyzes the velocity, temperature, and pressure distributions of a large area fire. The region of interest is the burning area. The analysis considers the effects of massive heating by combustion; the results presented are applicable to the lower surface layer. Predictions of the basic street-level environment can be made and above-shelter air temperatures can be defined. Coupled with an analysis of debris distributions and residual nuclear radiation (fallout or induced activity) in an attacked city, the velocity and temperature predictions will aid in defining the environment facing rescue forces.

This analysis differs considerably from previous treatments. No attempt is made to extrapolate results valid for a free-convection column. The theory presented directly relates the heat release of combustion and size of the burning area to calculated velocities and thermodynamic properties. The induced fire winds depend on the size of the fire and the combustion rate and are, to leading order, independent of the properties of the convective plume.

The results are restricted to large fires (small fires generate a different balance of forces than those considered here). The induced fire winds increase in intensity with heat release or fire size. Compressibility effects limit the maximum velocities attained; however, a continuous spectrum of fire-wind velocities is predicted, ranging from very low levels (corresponding to the experimental Flambeau fires) to high-velocity winds such as generated by the 1943 Hamburg firestorm.

It is clear that the fire is the forcing agent, and external influences are not needed to produce the devastating velocities encountered in the firestorms of World War II. If the fire persists long, swirl may slightly affect the high-velocity winds predicted here.

Sample calculations are presented for the largest Flambeau fires and for the Hamburg firestorm. The results agree with the documented observations and provide insight into the detailed hydrothermodynamic interactions occurring in a large area fire.

A nuclear weapon explosion can ignite fires over much larger areas than those covered by World War II firestorms. The theory developed in this report has been applied to large fires such as may occur in modern urban areas subject to megaton-yield explosions. Those results are presented in Part II of this report.

CONTENTS

PREFACE iii

SUMMARY v

FIGURES ix

SYMBOLS xi

Section
I. INTRODUCTION 1

II. ANALYSIS 3
Scalings and basic equations 6
Boundary conditions 8

III. SOLUTIONS 13
Closed-form solution for weakly heated flows 13
Numerical solution procedure 16

IV. RESULTS 18
Flambeau fires 18
Hamburg firestorm 25

V. DISCUSSION 30

REFERENCES 33

FIGURES

1. Schematic of large-fire environment 4
2. Velocity field for multiple-fuel-bed Flambeau fire 20
3. Temperature contours for multiple-fuel-bed Flambeau fire 21
4. Pressure contours for multiple-fuel-bed Flambeau fire . 21
5. Horizontal velocity profiles for multiple-fuel-bed Flambeau fire 23
6. Vertical velocity profiles for multiple-fuel-bed Flambeau fire 23
7. Center-line temperature variation for multiple-fuel-bed Flambeau fire 24
8. Center-line velocity variation for multiple-fuel-bed Flambeau fire 24
9. Velocity field for Hamburg firestorm 27
10. Temperature contours for Hamburg firestorm 28
11. Pressure contours for Hamburg firestorm 28
12. Horizontal velocity profiles for Hamburg firestorm 29
13. Vertical velocity profiles for Hamburg firestorm 29

SYMBOLS

A, B = dimensionless constants

c_p = specific heat capacity at constant pressure

e = measure of numerical solution error

E = error tolerance

$\mathcal{E}_1$, $\mathcal{E}_2$ = effective turbulent kinematic viscosities

$\mathfrak{F}$ = functional form for ground-level thermal boundary condition

g = gravitational acceleration

H = maximum height of flames

H_c = scale height of convection column

k^* = reciprocal of graybody radiation mean free path

k_1, k_2 = effective turbulent thermal conductivities

K_1, K_2 = dimensionless heat-diffusion coefficients

M_1, M_2 = dimensionless momentum-diffusion coefficients

P = perturbation pressure (dimensionless)

$\hat{P}$ = pressure

P_a = ground-level atmospheric pressure in far field

P_1 = leading-order perturbation pressure for $\nu \ll 1$

P_{old}, P_{new} = successive values of P in numerical solution iterations

q, q_1 = dimensionless spatial distributions of volumetric heat-addition rate

Q = volumetric heat-addition-rate scale

r = radial position coordinate (dimensionless[†])

R = fire radius

T = temperature (dimensionless[†])

T_a = ground-level atmospheric temperature in far field

T_1 = leading-order perturbation temperature for $\nu << 1$

u = radial velocity (dimensionless[†])

u_1 = leading-order horizontal velocity for $\nu << 1$

U = radial velocity scale

v = vertical velocity (dimensionless[†])

v_1 = leading-order vertical velocity for $\nu << 1$

w = generic jump condition variable

y = vertical position coordinate (dimensionless[†])

$\tilde{y}$ = rescaled vertical coordinate

y_{max} = maximum y-value considered in numerical solution

γ = specific heat ratio

δ = dimensionless constant

ΔR = difference between maximum and minimum convection column radii in turning region

ε = reciprocal of combustion-zone aspect ratio

ν = dimensionless measure of volumetric heat-addition rate

ρ = density (dimensionless[†])

ρ_a = ground-level atmospheric density in far field

σ = dimensionless constant

$\hat{\sigma}$ = Stefan's constant

ω = relaxation coefficient

[†] Except in Eq. (3).

I. INTRODUCTION

Most previous analyses of free-burning fires have focused on the physics of the buoyant plume. The theories are restricted to small fires and are applicable only well above the flaming region. This report considers a large burning area and analyzes the strong-interaction region in and around the fire.

The buoyant plume above a small, free-burning fire is well described by integral theories that relate a sustained vertical flow to a weakly compressible gas state [Morton, Taylor, and Turner, 1956]. Dynamic pressure forces are assumed negligible, and a weak entrainment of ambient air is postulated at an effective plume edge. In and around the burning zone, however, such theories have limited applicability. The combustion processes foster large changes in temperature and density. Those changes create a region of strong buoyancy and hence nonnegligible pressure gradients.

Further, analysis of measurements [Cox and Chitty, 1980] shows that entrainment criteria fail to accurately describe the flow field at and just above the fire periphery. The horizontal velocity appears to decay inversely with height above the ground, and approaches a variation proportional to the center-line vertical velocity only well above the fire. It is the buoyancy-generated pressure forces, and not diffusive entrainment, that control the low-level induction of ambient air into the fire. The relationship between dynamic pressure and induced fire winds is indicated in the calculations of Smith, Morton, and Leslie [1975], though they assume that density changes are small (Boussinesq approximation) and do not seek fine resolution near the fire.

A model of the strongly buoyant flow generated in and around a large area fire is developed in Sec. II, producing a more highly resolved description of the mechanics of fire-wind generation. A "large area fire" is defined here as one of large aspect ratio, i.e., with much larger horizontal than vertical dimensions. The analysis is thus applicable to fires ranging in size from the multiple-fuel-bed Flambeau experiments [Countryman, 1969] to city-scale fires arbitrarily larger than those occurring in World War II [Bond, 1951; Irving, 1963; Middlebrook, 1981].

Attention is focused on the hydrothermodynamic processes in and around the combustion zone, and an uncoupled boundary-value problem describing the nonlinear relationships between heat addition, strong buoyancy, and pressure gradients is developed. The induced fire winds are related to the characteristics of the combustion zone through jump conditions applicable at the fire periphery. The specification of local boundary conditions enables one to predict fire winds without extensive numerical computations involving regions far from the combustion zone [Smith, Morton, and Leslie, 1975], and a much more detailed view of the burning-zone physics is made possible.

In one parameter limit, the model equations can be solved in closed form. The resulting solution concisely describes the basic interchanges of energy and momentum as well as the role of pressure gradients in fire-wind generation. Volume heating due to the combustion processes raises the gas temperature, lowers its density, and creates buoyancy. The pressure in and around the fire zone is then hydrostatically lowered, inducing the fire winds. That inflow is kinematically turned upward, forming the initial part of a convection column (plume) over the fire.

This analysis predicts that a nominal scale for the fire-wind inrush velocity varies linearly with fire size (width) and intensity (mean rate of heat release). For the multiple-fuel-bed Flambeau experiments and for the World War II Hamburg firestorm, velocity scales of about 9 and 18 m/sec, respectively, are predicted. Those values agree well with reported data [Countryman, 1969; Middlebrook, 1981]. Simulations of the near-fire velocity and thermodynamic fields induced by those events have been performed, and are presented in Sec. IV. Again, computed results duplicate observed flow patterns and are consistent with reported data.

II. ANALYSIS

The basic features and geometry of a large area fire system are illustrated in Fig. 1. The fuel bed may be either continuous or composed of discrete packets. However, it extends far enough that turbulence breaks the flame envelope, tending to keep flame heights uniform [Thomas, 1963]. Ambient air is drawn into the fire by a combination of physical processes involving heat addition, buoyancy, and pressure gradients. Air is heated in the combustion zone and rises buoyantly, carrying the products of combustion, to form a convection column. As cooler air replaces the rising, heated air, a high-speed inflow is produced in a surface layer that includes the lowest part of the convection column as well as the entire combustion zone. The portion of that layer that extends the width of the combustion zone is here called the turning region.

The present analysis examines the hydrothermodynamics of the turning region. In doing so, it also provides the initial conditions--vertical velocity and density difference from ambient--required for treatment of the convection column flow.

The turning-region flow is taken to be quasi-steady and axisymmetric. In Fig. 1, R represents the fire radius, H the maximum flame height, ΔR the difference between the maximum and minimum radii attained by the convection column in the turning region, and H_c a scale height for the column. For large area fires, $H \ll R$. A characteristic combustion-zone aspect ratio ε^{-1} is defined by

$$\varepsilon = \frac{H}{R} \ll 1 \ . \tag{1}$$

It has been observed that the column radius of a large fire decreases just slightly with height in the first five to fifteen flame heights, then increases slightly with altitude [U.S. Forest Service, 1967]. The initial decrease in radius can be associated with the strong fire-wind convection, so the height ("pinch point") at which the radius

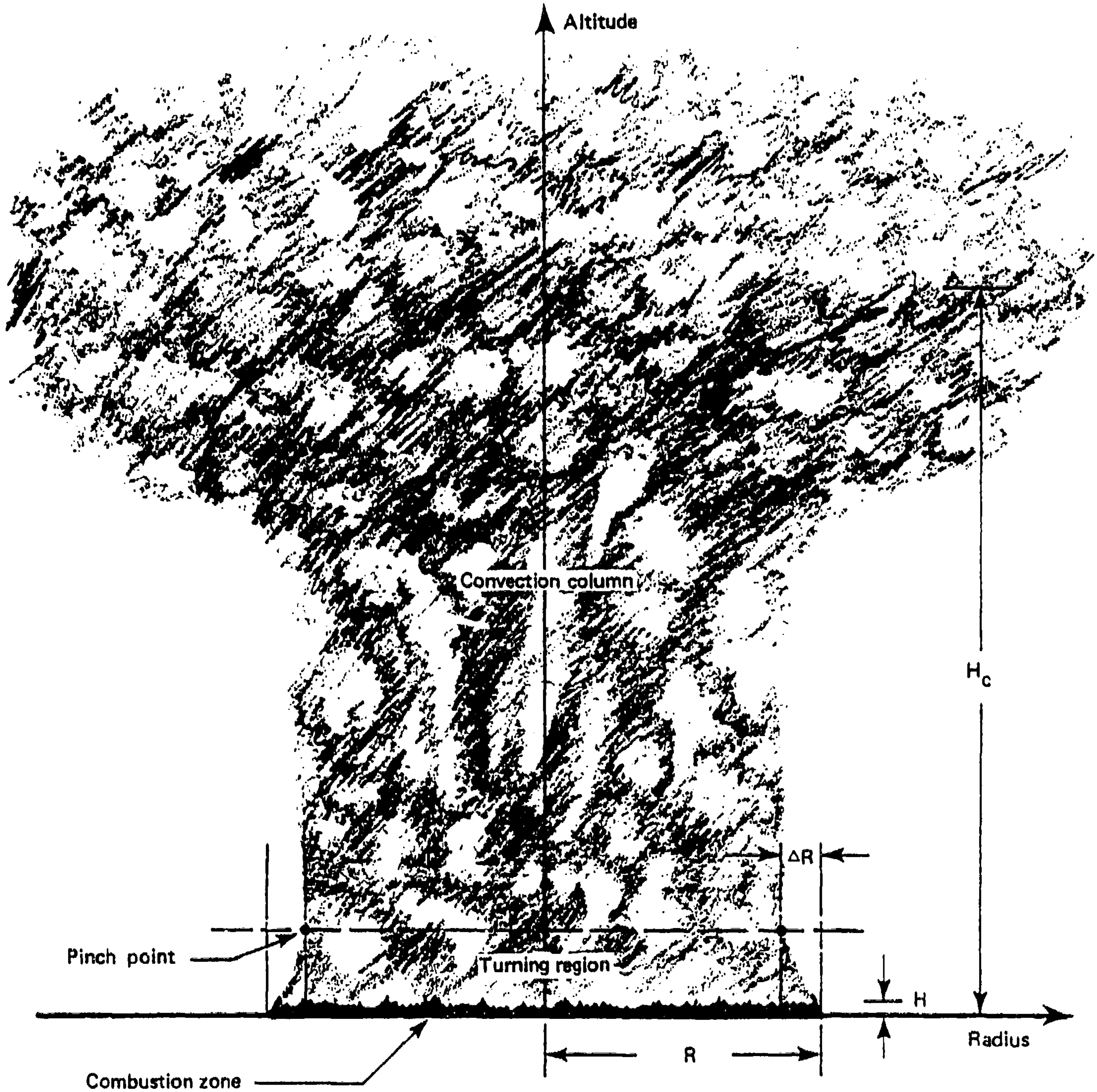

Fig. 1--Schematic of large-fire environment

first begins to increase provides a reasonable measure of the effective height of the turning region. In the model, it is thus assumed that that height is O(H) and

$$\Delta R << R \quad . \tag{2}$$

The net effect of the combustion processes is modeled as a spatially dependent rate of heat addition. The basic flow and thermodynamics of the turning region are thus decoupled from the specifics of those processes, and the complexities of detailed combustion modeling avoided. Changes in gas composition during combustion are also assumed negligible, but the Boussinesq approximation is not employed because large changes in temperature and density are expected. The flow in the turning region is thus taken to be that of an ideal, compressible gas undergoing heating in a finite zone at the bottom of the region.

There is some conjecture that, after long periods of time, ambient vorticity may be sufficiently concentrated to engender a rotating or swirling column [Long, 1967]. The rotation would in turn apply a biasing radial pressure gradient on the burning region and thus affect the rate of airflow into the fire. However, only a few observations support that hypothesis [Carrier, Fendell, and Feldman, 1982]. Therefore, rotational forces are neglected in our analysis.

The experimental work of McCaffrey [1979] and the analyses of Murgai [1962] and Smith [1967] suggest that radiation from the heated gas and attendant smoke plays an important role in reducing local air temperatures to nearly atmospheric within a few flame heights above the fire. Radiation losses as well as the effects of turbulent mixing are therefore included in the model, though in rather simple, qualitative ways. The radiation losses are assumed to occur in volume and to be graybody, or "transparent" [Murgai, 1962]. Eddy diffusivities are used to describe the Reynolds stresses.

At the fire periphery (radius $\approx$ R), steep gradients in temperature, pressure [Smith, Morton, and Leslie, 1975], and mixing coefficients are to be expected. Though they occur over distances much less than R, such rapid changes are critical in determining the more gradual variations over the entire width of the turning region. To account for them in the model, the following assumptions are also made. Since $\Delta R << R$, the radius of the turning region is taken to be R at all altitudes, and rapid changes in quantities around the periphery are idealized as jumps (discontinuities) at that radius. The magnitudes of such jumps are governed by standard statements of mass, momentum, and energy conservation. Outside the fire, the thermodynamic state is assumed to be that of the ambient atmosphere and turbulent stresses are taken to be much less than those inside.

SCALINGS AND BASIC EQUATIONS

We seek leading-order predictions of the mean horizontal and vertical velocity u and v, temperature T, density ρ, and pressure $\hat{P}$ in the turning region. The following nominal variable scalings (denoted by braces) are employed:

$$\{r\} = R \ , \qquad \{y\} = H \ ,$$

$$\{u\} = U \ , \qquad \{v\} = \epsilon U \ ,$$

$$\{T\} = T_a \ , \qquad \{\rho\} = \rho_a \ , \qquad \{\hat{P}\} = P_a \ , \tag{3}$$

where r and y represent radial and vertical position, respectively; U is a horizontal velocity scale yet to be chosen; and T_a, ρ_a, and P_a represent ground-level atmospheric temperature, density, and pressure.

Since a subsonic flow is expected, we rescale pressure using

$$\frac{\hat{P}}{P_a} = 1 + \delta P \ , \qquad \delta = \left(\frac{U^2}{P_a/\rho_a}\right) \ , \tag{4}$$

and anticipate that $\delta << 1$. Subject to this rescaling, the leading-order set of conservation and state equations is then found [Small, Larson, and Brode, 1981] to be

$$\frac{\partial}{\partial r}(r\rho u) + \frac{\partial}{\partial y}(r\rho v) = 0 \ , \tag{5a}$$

$$\rho\left(u\frac{\partial u}{\partial r} + v\frac{\partial u}{\partial y}\right) = -\frac{\partial P}{\partial r} + M_1\left(\frac{1}{r}\frac{\partial}{\partial r}\left(r\frac{\partial u}{\partial r}\right) - \frac{u}{r^2}\right) + M_2\frac{\partial^2 u}{\partial y^2} \ , \tag{5b}$$

$$\frac{\partial P}{\partial y} + A\rho = 0 \ , \tag{5c}$$

$$\rho\left(u\frac{\partial T}{\partial r} + v\frac{\partial T}{\partial y}\right) = B\left(q(r,\ y) - \sigma(T^4 - 1)\right)$$

$$+ K_1\left(\frac{1}{r}\frac{\partial}{\partial r}\left(r\frac{\partial T}{\partial r}\right)\right) + K_2\frac{\partial^2 T}{\partial y^2} \ , \tag{5d}$$

$$\rho T = 1 \ , \tag{5e}$$

where

$$A = \frac{gH}{U^2} \ ,$$

$$B = \frac{\gamma - 1}{\gamma}\left(\frac{QR}{P_a U}\right) \ ,$$

$$M_1 = \frac{\varepsilon \mathcal{E}_1}{\rho_a UH} \ , \qquad M_2 = \frac{\mathcal{E}_2}{\varepsilon \rho_a UH} \ ,$$

$$K_1 = \frac{\varepsilon k_1}{c_p \rho_a UH} \ , \qquad K_2 = \frac{k_2}{c_p \varepsilon \rho_a UH} \ ,$$

$$\sigma = 4\pi\hat{\sigma}k^* \frac{T_a^4}{Q} = 4\pi\hat{\sigma}T_a^4\left(\frac{k^* H}{QH}\right) \ . \tag{6}$$

Here, Q is a scale for the rate of heat addition due to combustion and $q(r,\ y)$ a specified spatial distribution. The $\mathcal{E}_i$ and k_i are dimensional mixing coefficients, the specific heat capacity c_p is assumed constant, $\hat{\sigma}$ is Stefan's constant, and k^* is the reciprocal of the radiation mean free path (assumed constant).

An appropriate value for the horizontal velocity scale U is found by balancing the terms for convective transport and heat addition in the energy equation so as to properly represent the physics of a flow driven by combustion heating. Accordingly, we take B = 1 and find the characteristic fire-wind velocity to be

$$U = \frac{\gamma - 1}{\gamma}\left(\frac{QR}{P_a}\right) \equiv \frac{\gamma - 1}{\gamma}\left(\frac{QH}{P_a \varepsilon}\right) \quad . \tag{7}$$

For the sample fires considered in Sec. IV, typical areal heating rates (QH) and burning-zone aspect ratios (ε^{-1}) are on the order of 5×10^4 cal/m^2-sec and 20, respectively. The characteristic velocity scales are thus of order 10 m/sec.

BOUNDARY CONDITIONS

The type of boundary conditions to be used with Eqs. (5) depends on the basic nature of the energy and horizontal momentum equations, and hence on the relative magnitudes of the coefficients M_i and K_i, $i = 1, 2$. A general model of turning-region turbulence might assume all such coefficients to be of numerical order one. The energy and horizontal momentum equations would then be elliptic. Special cases arise, however, when $M_1, K_1 \ll M_2, K_2 \sim O(1)$ or $M_2, K_2 \ll M_1, K_1 \sim O(1)$. Equations (5b) and (5d) are then nearly parabolic, and it is more appropriate to consider a parabolic analysis than a fully elliptic one. In this subsection, we discuss the boundary conditions required for each type of analysis.

We consider first the elliptic case, where all mixing coefficients are of order one. The flow must satisfy a no-slip condition at the ground, and a temperature condition must also be enforced. That is,

$$u = v = 0 \ , \qquad \mathcal{F}\left(T, \frac{\partial T}{\partial y}\right) = 0 \qquad \text{on } y = 0 \ , \tag{8}$$

where $\mathcal{F} = 0$ prescribes either a heat loss to the ground or a temperature distribution. Symmetry at the axis requires

$$u = \frac{\partial T}{\partial r} = 0 \qquad \text{on } r = 0 \ . \tag{9}$$

For the flow in the upper part of the turning region to be of the nearly vertical, weakly buoyant type characteristic of the convection column, it is further necessary that, to leading order,

$$u \to 0 \ , \qquad T \to 1 \ , \qquad P + Ay \to 0 \qquad \text{as } y \to \infty \ . \tag{10}$$

The conditions in Eqs. (10) are formally derived [Small, Larson, and Brode, 1981] from a matching of asymptotic expansions that describe, as $\varepsilon \to 0$, the separate turning-region and convection-column flows. Since H is much less than the atmospheric scale height, we take the ambient temperature and pressure outside the turning region to be $T_a(1 + o(1))$ and $P_a(1 + \delta Ay(1 + o(1)))$, respectively [see Eqs. (3) and (4)].

Finally, in order to conserve mass, momentum, and energy across the fire perimeter ($r = 1$), the magnitudes of effective jumps in physical quantities at $r = 1$ must satisfy certain conditions. Those jump conditions are easily found by writing Eqs. (5a), (5b), and (5d) in conservation form and then integrating them from $r = 1^-$ to 1^+. With the jump ($r = 1^-$ to 1^+) being denoted by $[w]$, the resulting conditions† are

$$[\rho u] = 0 \ ,$$

$$[\rho u^2] = -[P] + \left[M_1 \frac{\partial u}{\partial r}\right] \ ,$$

$$[\rho u T] = \left[K_1 \frac{\partial T}{\partial r}\right] \ . \tag{11}$$

†Since Eq. (5c) contains no r-derivative, the analogous jump condition is trivially satisfied and a consistent leading-order description is maintained.

To leading order, with mixing coefficients being much greater inside the turning region than outside, and atmospheric temperature being $T_a(1 + o(1))$, we have

$$T^+ = \rho^+ = 1 \ , \qquad \left[M_1 \frac{\partial u}{\partial r}\right] = M_1^- \left(\frac{\partial u}{\partial r}\right)^- \ , \qquad \left[K_1 \frac{\partial T}{\partial r}\right] = K_1^- \left(\frac{\partial T}{\partial r}\right)^- \ , \quad (12)$$

where $T^+ = T\big|_{r=1^+}$, etc. Thus, by integrating Eq. (5c) along $r = 1^+$,

$$P^+ = -Ay \ . \quad (13)$$

Using Eqs. (12) and (13), we can rewrite the jump conditions in Eqs. (11) as

$$u^+ = \rho u \ ,$$

$$M_1 \frac{\partial u}{\partial r} - (P + Ay) = \rho u^2 - (u^+)^2 \ ,$$

$$K_1 \frac{\partial T}{\partial r} = u - u^+ \ , \quad (14)$$

where nonsuperscripted variables represent values at $r = 1^-$. Substituting the first equality here into the second and the third, then using Eq. (5e), we find the following boundary conditions to be applicable at the fire periphery:

$$M_1 \frac{\partial u}{\partial r} = \left(\frac{u}{T}\right)^2 (T - 1) + (P + Ay) \ , \qquad K_1 \frac{\partial T}{\partial r} = \frac{u}{T} (T - 1)$$

$$\text{on } r = 1 \ . \quad (15)$$

The primarily elliptic boundary-value problem posed by Eqs. (5), (8), (9), (10), and (15) provides a model for the hydrothermodynamics of the turning region in the case where all M_i and K_i are of numerical order one. That model thus describes flows for which the effects of turbulent mixing are dynamically important in both horizontal and vertical directions.

We now consider the nearly parabolic case where M_1, $K_1 << M_2$, K_2, which is characteristic of flows having a vertically dominant turbulent structure. In a fully parabolic analysis with $M_1 = K_1 = 0$, the boundary conditions in Eqs. (8) and (10) must be retained, but the symmetry conditions in Eq. (9) cannot be imposed. In general, those symmetry conditions can be satisfied only through the development of an axial boundary layer in which horizontal mixing again plays a leading-order role. Additionally, the two jump conditions in Eqs. (15) degenerate for $M_1 = K_1 = 0$ to the single condition $T = 1$. With no peripheral constraint being imposed on u, the parabolic analysis cannot yield a unique determination of the turning-region flow.

The other nearly parabolic case occurs for flows having a horizontally dominant turbulent structure, i.e., where M_2, $K_2 << M_1$, K_1. A developing column flow has such a structure. In a fully parabolic analysis with $M_2 = K_2 = 0$, all boundary conditions in Eqs. (9) and (15) must be retained, so as to preserve the correct flow structure about the symmetry axis and at the fire perimeter. However, along $y = 0$, neither the no-slip condition on velocity nor any condition on temperature can be enforced. The satisfaction of those conditions [Eqs. (8)] requires the development of a thin surface layer in which vertical mixing plays an important role. Further, the only necessary condition in Eqs. (10) is that involving pressure. As Eqs. (5c) and (5e) imply, ρ and $T \to 1$ as $y \to \infty$ if $P + Ay \to 0$. Thus, from Eqs. (5b), (9), and (15), $u \to 0$ in that limit. The proper set of boundary conditions for the case where $M_2 = K_2 = 0$ is therefore

$$v = 0 \qquad \text{on } y = 0 , \tag{16a}$$

$$u = \frac{\partial T}{\partial r} = 0 \qquad \text{on } r = 0 , \tag{16b}$$

$$P + Ay = 0 \qquad \text{as } y \to \infty \ , \tag{16c}$$

and

$$M_1 \frac{\partial u}{\partial r} = \left(\frac{u}{T}\right)^2 (T - 1) + (P + Ay) \ , \qquad K_1 \frac{\partial T}{\partial r} = \frac{u}{T} (T - 1)$$

$$\text{on } r = 1 \ . \tag{16d}$$

With the exception of a thin, viscous layer near the ground, the parabolic flow model defined for M_2, $K_2 = 0$ by Eqs. (5) and (16) retains the basic physical features and structure of the earlier elliptic model. The resulting boundary-value problem is a local one: its solution provides a prediction of the near-fire environment and the corresponding fire winds without additional analysis of the far field. The remaining sections present solutions and results for that parabolic case.

III. SOLUTIONS

CLOSED-FORM SOLUTION FOR WEAKLY HEATED FLOWS

Before considering the general numerical solution of Eqs. (5) and (16) for M_2, $K_2 = 0$, it is instructive to examine the restricted case of a "weakly heated" flow, i.e., q(r, y) small. A representative closed-form solution that summarizes the physical interactions in the turning-region flow is derived using the following:

$$q(r,\ y) = \nu q_1(y)\ ,$$

$$q_1(y) = \begin{Bmatrix} 1 & \text{for} & 0 \le y \le 1 \\ 0 & \text{for} & y > 1 \end{Bmatrix}\ ,$$

$$\nu \ll 1\ . \tag{17}$$

For weak heating, relatively small temperature changes and velocities are expected. Asymptotic expansions of the following type, valid as $\nu \to 0$, are thus sought for the solution of Eqs. (5) and (16):

$$T \sim 1 + \nu T_1 + \cdots\ , \tag{18a}$$

$$\rho \sim 1 - \nu T_1 + \cdots\ , \tag{18b}$$

$$P \sim -Ay + \nu P_1 + \cdots\ , \tag{18c}$$

$$u \sim \nu u_1 + \cdots\ , \tag{18d}$$

$$v \sim \nu v_1 + \cdots\ . \tag{18e}$$

In the $\nu \to 0$ limit, the leading-order problem obtained by substituting Eqs. (17) and (18) into Eqs. (5) and (16) is then

$$K_1\left(\frac{1}{r}\frac{\partial}{\partial r}\left(r\,\frac{\partial T_1}{\partial r}\right)\right)+\left(q_1(y)-4\sigma T_1\right)=0\ , \tag{19a}$$

$$\frac{\partial P_1}{\partial y}=AT_1\ , \tag{19b}$$

$$M_1\left(\frac{1}{r}\frac{\partial}{\partial r}\left(r\,\frac{\partial u_1}{\partial r}\right)-\frac{u_1}{r^2}\right)=\frac{\partial P_1}{\partial r}\ , \tag{19c}$$

$$\frac{\partial v_1}{\partial y}=-\frac{1}{r}\frac{\partial}{\partial r}\,(ru_1)\ , \tag{19d}$$

subject to

$$v_1=0 \qquad \text{on } y=0\ , \tag{20a}$$

$$u_1=\frac{\partial T_1}{\partial r} \qquad \text{on } r=0\ , \tag{20b}$$

$$P_1\to 0 \qquad \text{as } y\to\infty\ , \tag{20c}$$

$$M_1\,\frac{\partial u_1}{\partial r}=P_1\ , \qquad \frac{\partial T_1}{\partial r}=0 \qquad \text{on } r=1\ . \tag{20d}$$

The problem posed by Eqs. (19) and (20) is readily solved. Equation (19a) involves T_1 alone. Subject to boundary conditions (20b) and (20d), it must have a solution that depends only on y. Once that solution is found, Eqs. (19b), (19c), and (19d) are decoupled and solved in succession for P_1, u_1, and v_1. For $y > 1$, $q_1(y) \equiv 0$. The only solution of Eqs. (19) then satisfying Eqs. (20b), (20c), and (20d) has T_1, P_1, u_1, and $\partial v_1/\partial y$ all zero. That is,

$$T_1\equiv P_1\equiv u_1\equiv 0\ , \qquad v_1\equiv v_1(r,\ 1) \quad \text{for} \quad y>1\ , \tag{21}$$

where the $v_1(r, 1)$ profile is yet to be found.

For $0 \leq y \leq 1$, $q_1(y) \equiv 1$ and it can be easily verified that the unique solution of the uncoupled boundary-value problem for T_1 is $T_1 \equiv 1/(4\sigma)$. Formally, then, the solution for T_1 suffers a discontinuity at $y = 1$. However, the discontinuity may be removed by using a boundary-layer-type solution about $y = 1$. With y stretched in this layer by

$$\tilde{y} = \frac{y - 1}{\nu} , \tag{22}$$

the leading-order versions ($\nu \to 0$) of Eqs. (5) become

$$v_1 \frac{\partial T_1}{\partial \tilde{y}} = K_1 \left(\frac{1}{r} \frac{\partial}{\partial r} \left(\frac{\partial T_1}{\partial r} \right) \right) + \left(q_1(y) - 4\sigma T_1 \right) ,$$

$$\frac{\partial P_1}{\partial \tilde{y}} = 0 ,$$

$$v_1 \frac{\partial u_1}{\partial \tilde{y}} = M_1 \left(\frac{1}{r} \frac{\partial}{\partial r} \left(r \frac{\partial u_1}{\partial r} \right) - \frac{u_1}{r^2} \right) - \frac{\partial P_1}{\partial r} ,$$

$$\frac{\partial v_1}{\partial \tilde{y}} = 0 . \tag{23}$$

An appropriate solution of this system provides the desired smooth transition in T_1 from $1/(4\sigma)$ as $\tilde{y} \to -\infty$, to zero as $\tilde{y} \to +\infty$. It is further clear from Eqs. (23) that P_1 and v_1 must be independent of $\tilde{y}$ over the boundary layer. The solution of Eqs. (19) for $0 \leq y \leq 1$ must therefore satisfy $P_1(r, 1) \equiv 0$, and provides the $v_1(r, 1)$ profile to be used for $y > 1$.

With $T_1 \equiv 1/(4\sigma)$ and $P_1(r, 1) = 0$, the complete solution of Eqs. (19) and (20) for the fire zone is then found to be

$$T_1 \equiv \frac{1}{4\sigma} ,$$

$$P_1 = - \frac{A}{4\sigma} (1 - y) ,$$

$$u_1 = \left(\frac{P_1}{M_1}\right) r = - \frac{A}{4\sigma M_1} (1 - y) r ,$$

$$v_1 = \frac{A}{2\sigma M_1} \left(y - \frac{y^2}{2}\right) \qquad \text{for } 0 \leq y \leq 1 . \tag{24}$$

This solution summarizes the basic turning-region physics. The combustion heating [Eq. (19a)] causes an increase in temperature and thus a decrease in density [Eq. (18b)]. The mean pressure is then hydrostatically lowered [Eq. (19b)], inducing the fire-wind inflow [Eq. (20d)]. Finally, the inflow is kinematically turned upward [Eq. (19d)], forming the initial part of the convection column.

NUMERICAL SOLUTION PROCEDURE

In general, the boundary value problem posed by Eqs. (5) and (16) must be solved by numerical computation. Subject to M_2, $K_2 = 0$, the differential equations in set (5) are either parabolic or first-order hyperbolic. Such equations are usually solved subject to initial conditions or certain combinations of initial and boundary conditions, but not subject to boundary conditions on all sides of the domain of definition, as prescribed by Eqs. (16). The boundary value problem is thus unusual, and a novel algorithm is employed to solve it numerically.

Our scheme involves iteration toward the correct form of $P(r, 0)$ [Small, Larson, and Brode, 1981]. For $y = 0$, we have $v \equiv 0$, and u, T, and P must satisfy the following ordinary-differential-equation boundary value problem:

$$\left(\frac{u}{T}\right)\frac{\partial u}{\partial r} = -\frac{\partial P}{\partial r} + M_1\left(\frac{1}{r}\frac{\partial}{\partial r}\left(r\frac{\partial u}{\partial r}\right) - \frac{u}{r^2}\right) ,$$

$$\left(\frac{u}{T}\right)\frac{\partial T}{\partial r} = q(r,\ 0) - \sigma(T^4 - 1) + K_1\left(\frac{1}{r}\frac{\partial}{\partial r}\left(r\frac{\partial T}{\partial r}\right)\right) ,$$

$$u = \frac{\partial T}{\partial r} = 0 \qquad \text{at } r = 0 ,$$

$$M_1\frac{\partial u}{\partial r} = \left(\frac{u}{T}\right)^2 (T - 1) + P , \qquad K_1\frac{\partial T}{\partial r} = \frac{u}{T}(T - 1)$$

$$\text{at } r = 1 . \tag{25}$$

First, a form is chosen for $P(r, 0)$, then $u(r, 0)$ and $T(r, 0)$ are predicted from a standard finite-difference solution of Eqs. (25). A nonlinear Crank-Nicolson scheme [Isaacson and Keller, 1966] is next used to obtain a numerical solution of Eqs. (5), (16a), (16b), and (16d) for $y > 0$. After the calculation is carried to some specified altitude $y_{max}(>>H)$, the error index $e = \max\limits_{0\le r\le 1}|P(r, y_{max}) + Ay_{max}|$ is computed [cf. Eq. (16c)]. If $e < E$, with E being a specified error tolerance, the solution procedure is completed. If $e > E$, a new form for $P(r, 0)$ is chosen using the following simple iteration scheme:

$$P(r,\ 0)_{new} = P(r,\ 0)_{old} - \omega\left(P(r,\ y_{max}) + Ay_{max}\right) , \tag{26}$$

where ω is a specified relaxation coefficient. The prediction steps are then repeated until the process converges with $e < E$.

In practice, the scheme has proved to be stable and convergent--subject, of course, to reasonable initial values for $P(r, 0)$. For $q(r, y)$ as in Eqs. (17), the resulting numerical solution reproduces the closed-form weak-heating solution in Eqs. (18), (21), and (24).

IV. RESULTS

FLAMBEAU FIRES

The multiple-fuel-bed Flambeau fires [Countryman, 1969; Palmer, 1981] were large, controlled burns conducted to simulate the characteristics of a fire that has simultaneously engulfed nearly all parts of an urban area. The fuel beds consisted of several hundred separated piles of mixed juniper and pinyon pine logs and cuttings. Each experiment was instrumented for temperature, velocity, and weight loss. Additionally, the fires were filmed to provide a permanent visual record.

The largest Flambeau fires covered areas of about 20 ha, had flames rising up to 20 m, and produced heat release rates on the order of 10^4 to 10^5 cal/m^2-sec [Countryman, 1969; Palmer, 1981]. Maximum heat release is thought to have occurred in and around the fuel zone (height $\sim$ 4 m), the heating decreasing with altitude above that zone. In simulating the largest Flambeau fires, we thus use†

$$R = 250 \text{ m} , \qquad H = 20 \text{ m} , \qquad QH = 5.7 \times 10^4 \text{ cal/m}^2\text{-sec} ,$$

$$q(r, y) = \left\{ \begin{array}{ll} 1.6 & \text{for} \quad 0 \le y \le 0.25 \\ 1.6 \left[\left(\frac{4}{3} \right) (1 - y) \right] & \text{for} \quad 0.25 \le y \le 1.0 \\ 0 & \text{for} \quad y \ge 1.0 \end{array} \right\} . \qquad (27)$$

From Eqs. (1), (4), (6), (7), and (27), we then have $\varepsilon = 0.08$, a horizontal fire-wind velocity scale of

---

†The specific value of QH here is suggested by Lommasson et al. [1968]. The specific form of q(r, y) is chosen to satisfy the normalization

$$\int_0^1 \int_0^1 rq(r, y)\, dr\, dy = 1/2 ,$$

which holds if $q \equiv 1$.

$$U = 8.41 \quad \text{m/sec} , \tag{28}$$

and

$$\delta = 9.04 \times 10^{-4} , \qquad A = 2.77 . \tag{29}$$

The required data set is completed by specifying a radiation mean free path k^{*-1} and turbulent mixing coefficients M_1 and K_1. Use of the graybody approximation [Murgai, 1962] assumes that $k^*H << 1$. However, Smith [1967] suggests that, for a turbulent flow, the effective absorption coefficient may be 30 to 80 times larger than the laminar absorption coefficient, implying that k^*H could be of order one or larger. Since measurements supporting estimates of that parameter are not available for the fires considered, we select the nominal value $k^*H = 1$. Thus, from Eqs. (27) and (6),

$$k^{*-1} = 20 \text{ m} \quad \text{and} \quad \sigma = 0.022 . \tag{30}$$

The one-parameter eddy-viscosity model of turbulence effects represents a gross simplification of the actual field turbulence. Because of a lack of reliable correlations or other relevant data, more detailed modeling does not seem warranted at this time. For that reason, we have performed calculations for several sets of eddy coefficients. The sample results we now present were developed for

$$M_1 = K_1 = 4.0 , \tag{31}$$

which corresponds to $\mathcal{E}_1/\rho_a U = 1000$ m.

The results of the Flambeau simulation are illustrated by the vector, contour, and profile plots in Figs. 2 through 8. The basic flow pattern predicted by the model analysis is diagrammed in Fig. 2. The temperature rise and subsequent pressure drop in and around the fire due to combustion heating are shown in Figs. 3 and 4, respectively. The temperature attains a maximum mean of 637°K at the center of the combustion zone. However, it then decreases rapidly with increasing height, attaining a state of weak buoyancy above an altitude of 100 m.

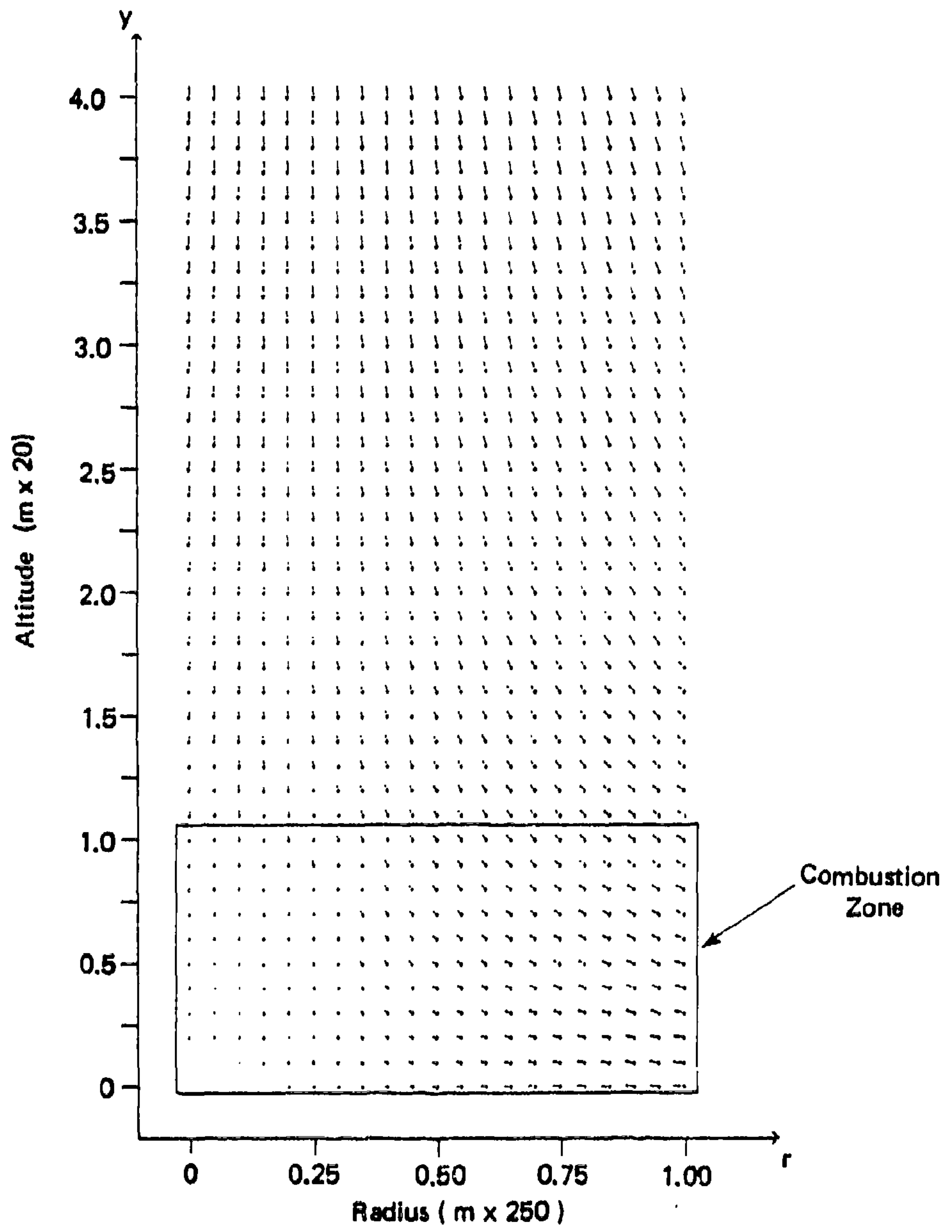

Fig. 2--Velocity field for multiple-fuel-bed Flambeau fire

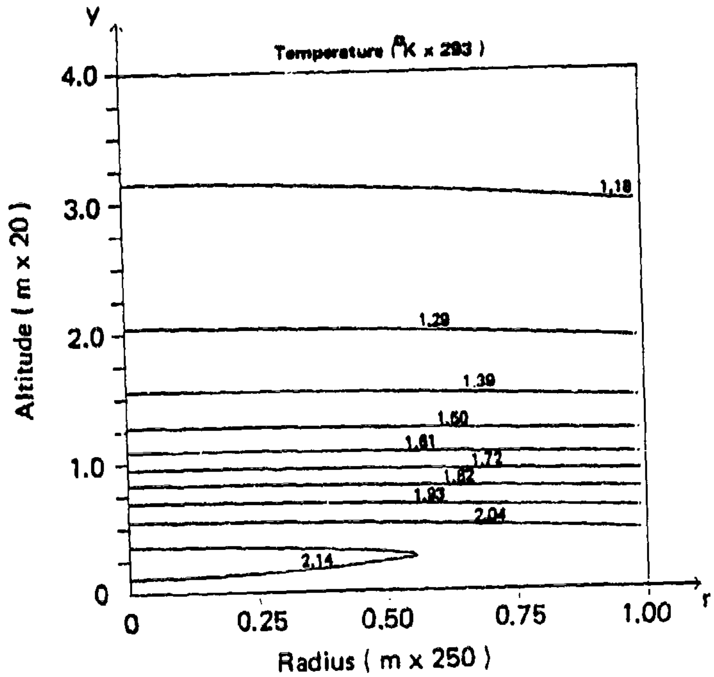

Fig. 3--Temperature contours for multiple-fuel-bed Flambeau fire

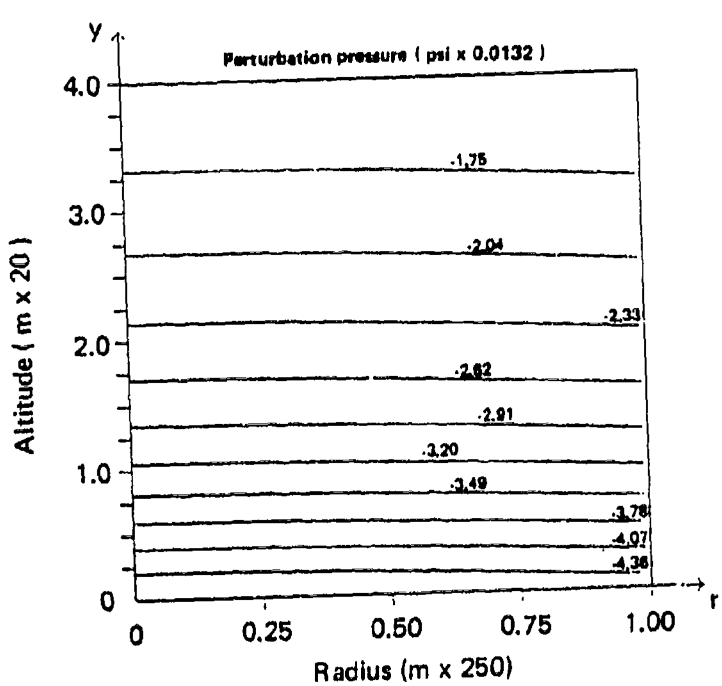

Note: Perturbation pressure is δp_s (P + Ay); see Eq. (4).

Fig. 4--Pressure contours for multiple-fuel-bed Flambeau fire

Pressure is almost independent of radial range except, of course, at the turning-region periphery. Such behavior is also characteristic of the more global computational results presented by Smith, Morton, and Leslie [1975]. The maximum pressure drop at the periphery occurs at ground level, and is 0.060 psi.

Figure 5 illustrates the basic nature of the horizontal inrush induced by the overall pressure drop. The maximum fire-wind inflow velocity at the periphery also occurs at ground level, and is 9.29 m/sec. The resultant upward flow consistent with the induced inflow is described in Fig. 6. Vertical velocity profiles are all nearly "top-hat," with $v \approx 4$ m/sec in the upper part of the turning region.

Figure 7 plots the center-line variation in temperature. In the heating zone, the temperature reaches a maximum and then decreases owing to radiative cooling of the hot gases. As $y \to \infty$, the temperature asymptotes to that of the ambient atmosphere. The center-line velocity variation in Fig. 8 shows a rapid, nearly linear increase in the turning region, then a slower increase with altitude. For $y \gtrsim 7$, the velocity approaches a constant value consistent with the initial convection column velocity. This behavior is similar to that observed for small fires [McCaffrey, 1979].

In general, quantitative comparisons of model predictions with Flambeau measurements are hindered by measurement scatter and the probability of error. However, a number of qualitative comparisons can realistically be made; in those cases, the predictions match the observed physical phenomena. For example, the basic flow pattern in Fig. 2 is consistent with filmed observations of the largest Flambeau fires [U.S. Forest Service, 1967]: the horizontal inflow is turned strongly upward, with a nearly vertical convection column flow beginning to form at several flame heights above the fire. Additionally, predicted inflow velocities at the periphery and predicted temperatures match well with (means of the) values reported for those fires [Countryman, 1969]. The peripheral fire-wind profile in Fig. 5 is also consistent with the filmed observations: below the pinch-point level (see Fig. 1), maximal inward smoke advection occurs at ground level, but decreases with increasing altitude.

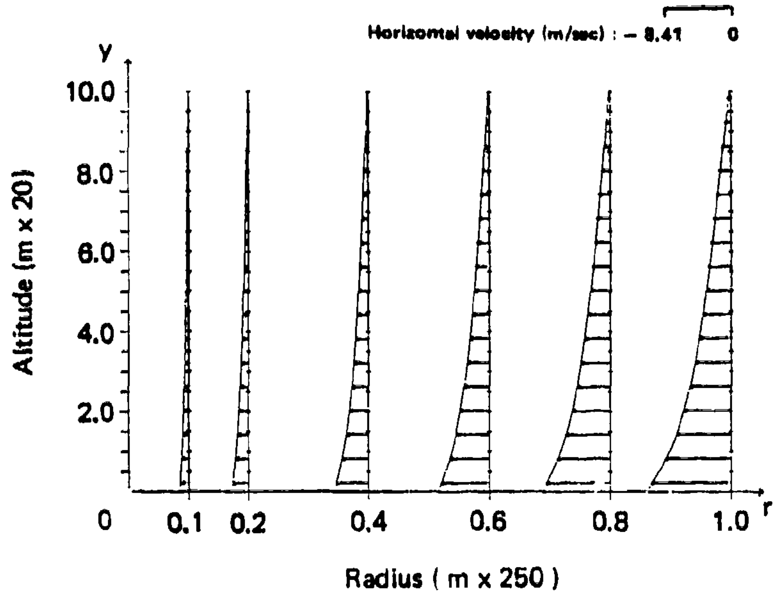

Fig. 5--Horizontal velocity profiles for multiple-fuel-bed Flambeau fire

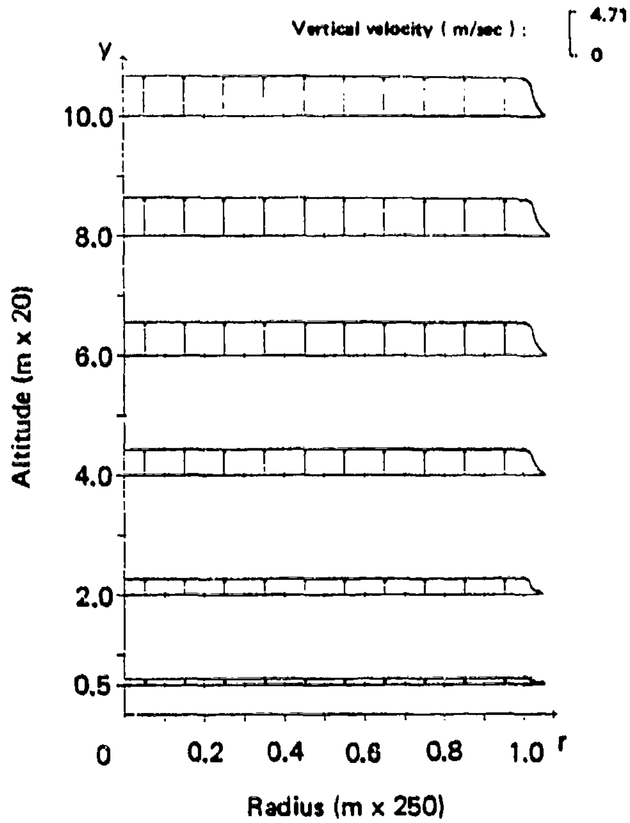

Fig. 6--Vertical velocity profiles for multiple-fuel-bed Flambeau fire

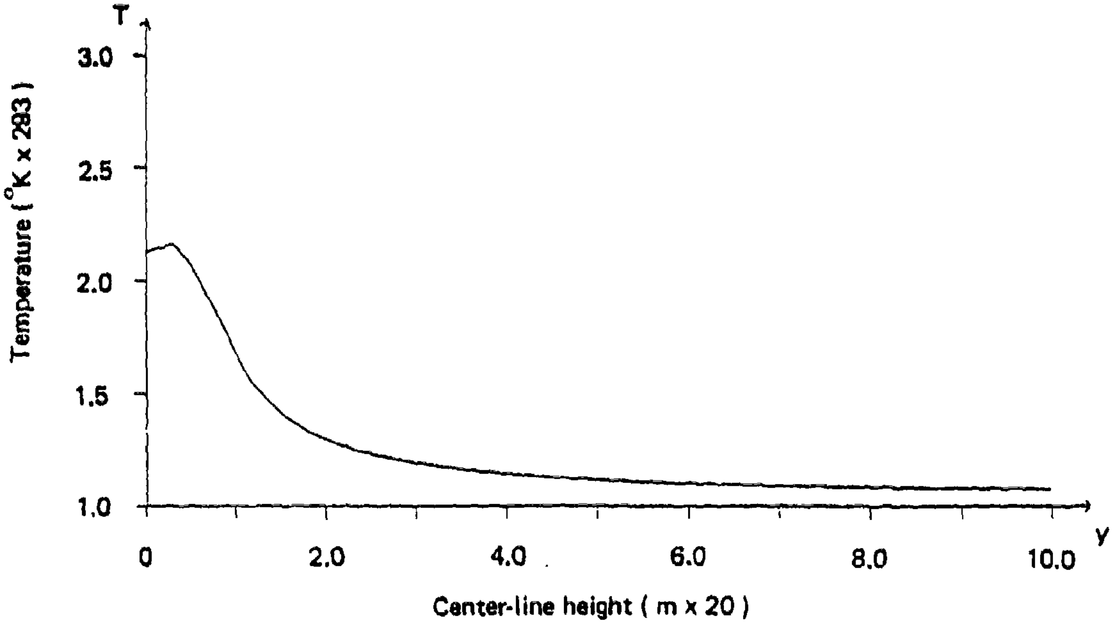

Fig. 7--Center-line temperature variation for multiple-fuel-bed Flambeau fire

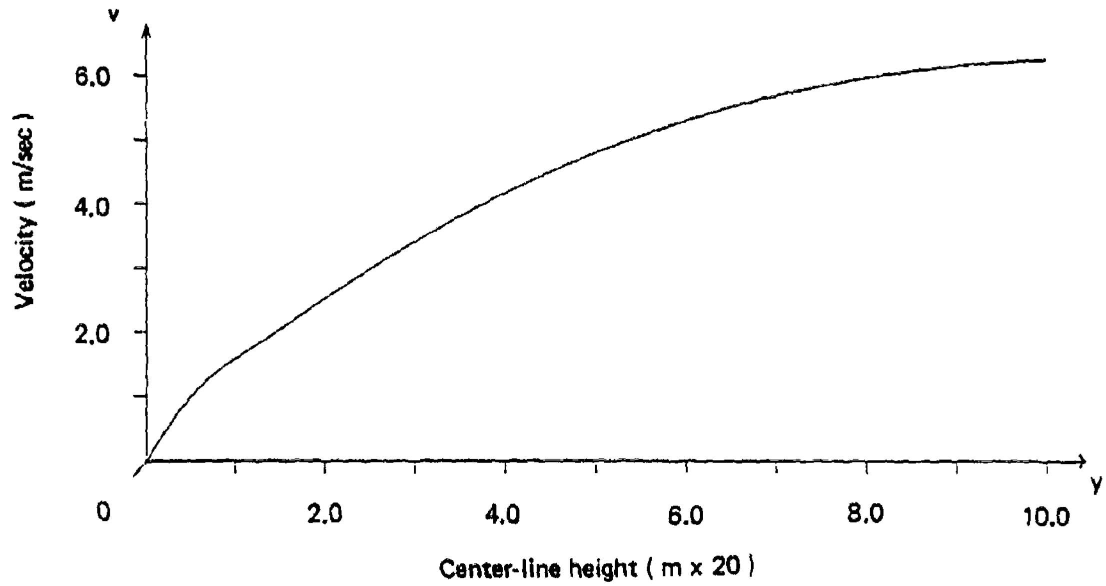

Fig. 8--Center-line velocity variation for multiple-fuel-bed Flambeau fire

HAMBURG FIRESTORM

The firestorm that devastated the Hammerbrook and Borgfelde districts of Hamburg in July 1943 [Middlebrook, 1981] was a result of unusually concentrated incendiary bombing. Those districts were largely residential, with densely packed, three- to six-story wood and masonry buildings providing the primary fuel bed. More technical data are available for this event than for other World War II firestorms; nevertheless, the data are limited.

In simulating the peak-period firestorm, we use

$$R = 1500 \text{ m}, \qquad H = 60 \text{ m}, \qquad QH = 5.7 \times 10^4 \text{ cal/m}^2\text{-sec} \tag{32}$$

[Lommasson et al., 1968; DCPA, 1973; Middlebrook, 1981]. Additionally, since the Hamburg fuel-zone height $\sim$ 15 m, we take $q(r, y)$ to be as in Eqs. (27). From Eqs. (1), (4), (6), (7), and (32), we then have $\varepsilon = 0.04$, a fire-wind velocity scale of

$$U = 16.8 \quad \text{m/sec}, \tag{33}$$

and

$$\delta = 3.61 \times 10^{-3}, \qquad A = 2.08 . \tag{34}$$

Consistent with our previous assumptions, we assume $k^{*-1} = 20$ m [cf. Eqs. (30)] and thus from Eqs. (6) find

$$\sigma = 0.066 . \tag{35}$$

Similarly, we performed model calculations for various sets of mixing coefficients and present results here for

$$M_1 = K_1 = 2.0 . \tag{36}$$

In general, the value of the eddy viscosity should reflect the eddy size as well as the magnitude of the mean flow. Intuitively, it is expected that the eddy size should increase with the fire radius. The change in parameter values between Eqs. (31) and (36) corresponds to a linear increase in $\mathcal{E}_1/\rho_a$ with radius.

The results of the Hamburg simulation are illustrated in Figs. 9 through 13. The temperature contours plotted in Fig. 10 show the effect of the combustive heating occurring in the burning zone. At the fire periphery ($r = 1$, $y \leq 1$), the temperature jumps from the ambient to a mean value consistent with the volume heating. In the lower portion of the burning region, the temperature increases as $r \rightarrow 0$. The center-line temperature is approximately 10 percent higher than the boundary temperature. The air temperature drops rapidly for $y > 1$ and falls to within 7 percent of the ambient at about 300 m above the ground. At that point, a well-developed vertical flow is established, representing the early stages of the convection column (see Fig. 9).

Figure 11 presents contours of constant perturbation pressure. In the lower portion of the turning region, radial pressure gradients are readily observed. The maximum pressure drop observed in the field is 0.118 psi. Above the burning zone, the radial pressure gradients are much smaller and the perturbation pressure decreases rapidly to zero.

Figures 12 and 13 display horizontal and vertical velocity profiles, respectively, for the turning region. The fire-wind velocity peaks (18.3 m/sec) at the inlet to the fire zone. The induced fire winds decrease rapidly above $y = 1$. As $y \rightarrow 10$, the induced horizontal velocity decreases toward zero, indicating that lower order terms in an expansion for u are needed to describe the subsequent entrainment of ambient air into the column. Classical plume theories relate that velocity to the vertical velocity at the column center line. As in the Flambeau simulation, profiles of vertical velocity (Fig. 13) are "top hat" in form. The maximum velocity predicted at the top of the turning region is 4.19 m/sec.

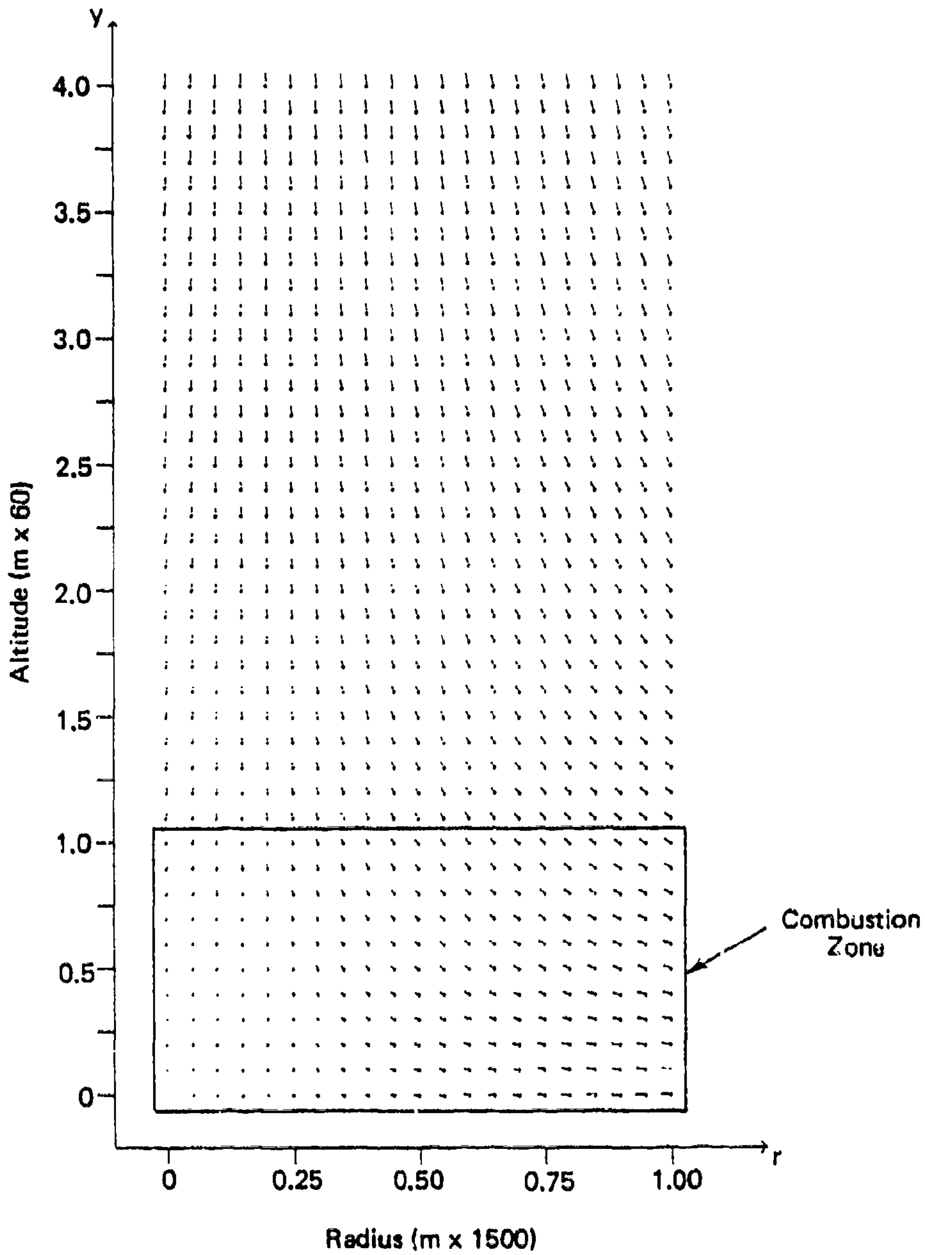

Fig. 9--Velocity field for Hamburg firestorm

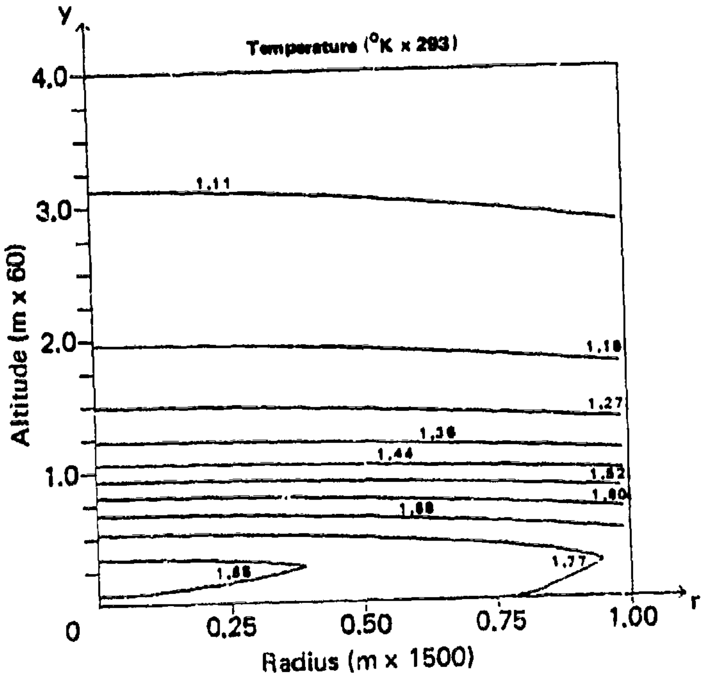

Fig. 10--Temperature contours for Hamburg firestorm

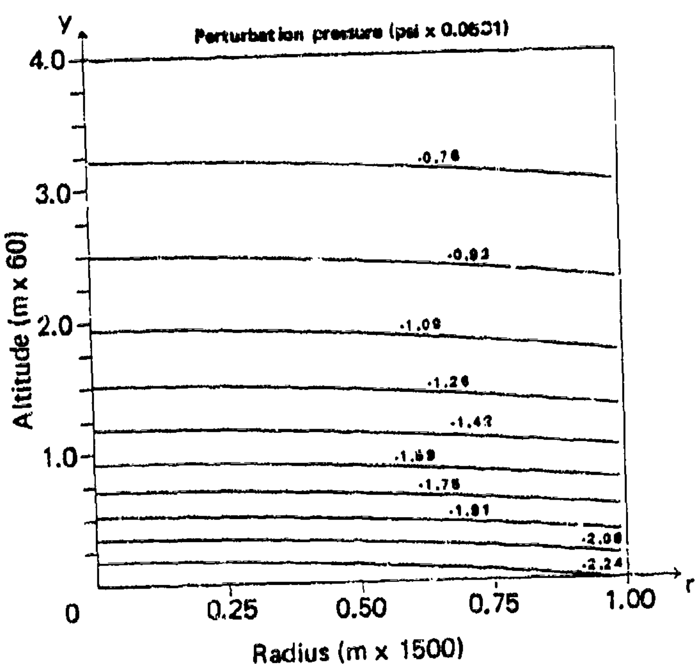

Note: Perturbation pressure is $\delta p_a (p + Ay)$; see Eq. (4).

Fig. 11--Pressure contours for Hamburg firestorm

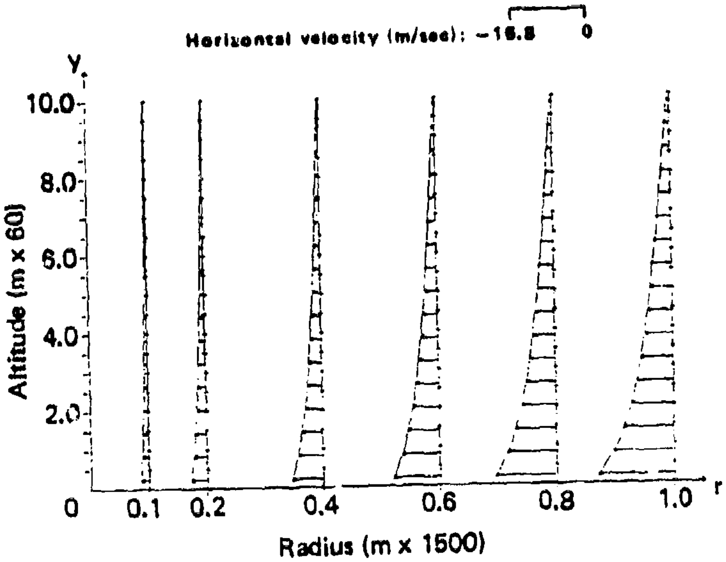

Fig. 12--Horizontal velocity profiles for Hamburg firestorm

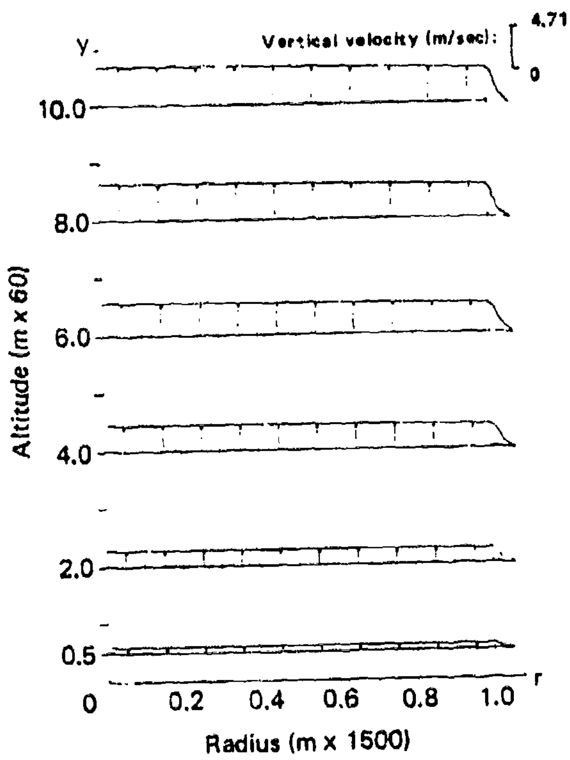

Fig. 13--Vertical velocity profiles for Hamburg firestorm

V. DISCUSSION

The model developed here describes the velocity and thermodynamic fields generated by a large urban fire. The analysis focuses on the turning region, which includes the burning zone and the region below the established free-convection column. Such an approach allows estimates to be made of the conditions necessary for shelter design and of the environment facing survivors and rescue workers. In addition, the results of the analysis provide insight into the complex interactions occurring in the turning region.

The analytical procedure employs asymptotic methods to simplify the basic equations of momentum and energy conservation. Such simplification allows one to consider the principal force balances while neglecting lower order effects. A finite-volume heat source is used to model the combustion processes, and large changes in temperature and density are allowed. A one-parameter eddy-viscosity model is used to describe the turbulent stresses, and a graybody approximation employed to model hot gas and smoke radiation. Jump conditions are derived to describe the rapid changes in physical quantities at the fire periphery. Those conditions effect model problem closure, allowing the induced fire winds to be calculated directly, without extensive far-field computations.

The use of one-parameter models to represent the combustion processes, turbulent exchanges, and radiative heat transfer simplifies the analytical formulation, but the models of course only approximate the complex physical phenomena. Further modeling could improve the approximations, but the current understanding of the turning-region hydrothermodynamics may not support a more rigorous analysis. In our sample simulations of the Flambeau fires and the Hamburg firestorm of 1943, observational data are used whenever possible to specify the model parameters. Parameters that cannot be defined from available data are allowed to vary over a range of values.

A closed-form solution to the relevant boundary-value problem is developed for the restricted case of weak heating. That solution reveals the structure of the general solution, and concisely shows how the heating, production of buoyancy, pressure gradients, induced fire winds, and formation of the initial free-convection column are related. Those relationships are also evident in the sample numerical simulations of the strongly heated Flambeau and Hamburg fires. At the fire periphery, the temperature increases rapidly, generating steep pressure gradients and high-velocity fire winds. The inrush is turned up by buoyancy all along the burning zone, and forms the base of a free-convection column in the upper portion of the turning region. The gas temperature increases slightly toward the center of the fire, but falls rapidly with height above the burning zone.

Finally, the model provides a flexible framework useful for further studies of the large-fire environment. For example, the solution defining the gas dynamic state provides information prerequisite to estimation of species concentrations. Leading-order versions of the conservation equations for each species can be developed [Small, Larson, and Brode, 1981] and solved to provide predictions of large-fire oxygen and noxious gas levels. The present analysis may also be extended to consider *time-dependent* heat release rates as long as they vary slowly over time periods characteristic of the resulting convection. Part II presents an example of such an extension.

REFERENCES

Bond, H. (ed.), *Fire and the Air War,* 1st ed., National Fire Protection Association, Boston, Massachusetts, 1951.

Carrier, G. F., F. E. Fendell, and P. S. Feldman, *Firestorms,* TRW Space and Technology Group, Redondo Beach, California, Document 38163-6001-UT-00, April 1982.

Countryman, C. M., *PROJECT FLAMBEAU . . . An Investigation of Mass Fire (1964-1967),* Vol. 1, U.S. Department of Agriculture, U.S. Forest Service, Berkeley, California, 1969.

Cox, G., and R. Chitty, "A Study of the Deterministic Properties of Unbounded Fire Plumes," *Comb. Flame,* Vol. 39, 1980, pp. 191-209.

DCPA Attack Environment Manual, Chap. 3, "What the Planner Needs To Know about Fire Ignition and Spread," U.S. Defense Civil Preparedness Agency and U.S. Department of Defense, Washington, D.C., June 1973.

Irving, D., *Destruction of Dresden,* Kimber, London, 1963.

Isaacson, E., and H. B. Keller, *Analysis of Numerical Methods,* Wiley, New York, 1966.

Long, R. R., "Fire Storms," *Fire Res. Abstr. Rev.,* Vol. 9, No. 2, 1967, pp. 53-68.

Lommasson, T. E., et al., *A "Firestorm" Existence and Buildup Hypothesis,* The Dikewood Corporation, September 1968.

McCaffrey, B. J., *Purely Buoyant Diffusion Flames: Some Experimental Results,* National Bureau of Standards, Washington, D.C., Report NBSIR79-1910, October 1979.

Middlebrook, M., *The Battle of Hamburg,* Scribner, New York, 1981.

Morton, B. R., G. I. Taylor, and J. S. Turner, "Turbulent Gravitational Convection from Maintained and Instantaneous Sources," *Proc. Roy. Soc. A.,* Vol. 24, 1956, pp. 1-23.

Murgai, M. P., "Radiative Transfer Effects in Natural Convections above Fires," *J. Fluid Mech.,* Vol. 12, 1962, pp. 441-448.

Palmer, T. Y., "Large Fire Winds, Gases and Smoke," *Atmos. Environment,* Vol. 15, No. 10/11, 1981, pp. 2079-2090.

Small, R. D., D. A. Larson, and H. L. Brode, *Analysis of Large Urban Fires,* Pacific-Sierra Research Corporation, Report 1122, September 1981.

Smith, R. K., "Radiation Effects on Large Fire Plumes," *Eleventh International Symposium on Combustion*, The Combustion Institute, Pittsburgh, 1967, pp. 507-515.

Smith, R. K., B. R. Morton, and L. M. Leslie, "The Role of Dynamic Pressure in Generating Fire Wind," *J. Fluid Mech.*, Vol. 68, 1975, pp. 1-19.

Thomas, P. H., "The Size of Flames from Natural Fires," *Ninth International Symposium on Combustion*, The Combustion Institute, Pittsburgh, 1963, pp. 844-859.

U.S. Forest Service, untitled films, Fire Laboratory, Riverside, California, 1967.

DISTRIBUTION LIST

National Addresses

Air Force Weapons Laboratory
Attn: Civil Engineering Division
Kirtland Air Force Base
Albuquerque, NM 87117 (1)

Air Force Weapons Laboratory
Attn: SUL Technical Library
Kirtland Air Force Base
Albuquerque, NM 87117 (1)

Mr. Raymond Alger
SRI International
Menlo Park, CA 94025 (1)

Mr. Norman J. Alvares
Lawrence Livermore National Laboratory
University of California
P.O. Box 808, L-442
Livermore, CA 94550 (1)

Assistant Director
Energy and Natural Resources
Office of Science and Technology Policy
Executive Office Building
Washington, D.C. 20500 (1)

Assistant Secretary of the Army (RD&A)
Attn: Deputy ASA for RD&S
The Pentagon
Washington, D.C. 20301 (1)

Dr. Jana Backovsky
SRI International
Menlo Park, CA 94025 (1)

Mr. A. P. Brackebush
Forest Fire Research
Northern Forest Fire Laboratory
Missoula, MT 59801 (1)

Mr. Clay P. Butler
SRI International
Menlo Park, CA 94025 (1)

Center for Planning and Research, Inc.
Attn: Document Library
2483 East Bayshore Road, Suite 104
Palo Alto, CA 94303 (1)

Dr. Craig Chandler, Director
Forest Fire & Atmospheric Science Research
U.S. Forest Service
Department of Agriculture
Washington, D.C. 20013 (1)

Dr. Conrad Chester
Oak Ridge National Laboratory
P.O. Box X
Oak Ridge, TN 37830 (1)

Chief of Engineers
Department of the Army
Attn: DAEN-RDZ-A
Washington, D.C. 20314 (1)

Dr. William F. Christian
Underwriters' Laboratories, Inc.
333 Pfingsten Road
Northbrook, IL 60062 (1)

Civil Engineering Center/AF/PRECET
Wright-Patterson Air Force Base, OH 45433 (1)

Dr. John Cockayne
Senior Scientist
Science Applications, Inc.
1710 Goodridge Drive
McLean, VA 22102 (1)

Defense Technical Information Center (DTIC)
Cameron Station
Alexandria, VA 22314 (12)

Department of Defense
Command and Control Technical Center
Attn: Office of the Director
The Pentagon
Washington, D.C. 20301 (1)

Department of Energy
Attn: Director, Department of Military Application
Washington, D.C. 20545 (1)

The Dikewood Corporation
Attn: Document Library
1613 University Boulevard, N.E.
Albuquerque, NM 87102 (1)

Director
Defense Nuclear Agency
Attn: Michael Frankel
Washington, D.C. 20305 (1)

Director
Defense Nuclear Agency
Attn: LtCol. David H. Thomas, USAF
Washington, D.C. 20305 (1)

Director
Lovelace Foundation
5200 Gibson Boulevard, S.E.
Albuquerque, NM 87108 (1)

Director, U.S. Army Ballistic Research Laboratory
Attn: Document Library
Aberdeen Proving Grounds, MD 21005 (1)

Director, U.S. Army Ballistic Research Laboratory
Attn: Mr. William Taylor
Aberdeen Proving Grounds, MD 21005 (2)

Director, U.S. Army Engineer Waterways Experiment Station
Attn: Document Library
P.O. Box 631
Vicksburg, MS 39180 (1)

Director, U.S. Army Engineer Waterways Experiment Station
Attn: Mr. W. L. Huff
P.O. Box 631
Vicksburg, MS 39180 (1)

Director, U.S. Army Materials and Mechanics Research Center
Attn: Technical Library
Watertown, MA 02172 (1)

Mr. Marvin Drake
Science Applications, Inc.
1250 Prospect Street
La Jolla, CA 92037 (1)

Mr. Donald Drzewiecki
Calspan Corporation
P.O. Box 400
Buffalo, NY 14225 (1)

Factory Mutual Research Corporation
Attn: Dr. Ray Friedman
1151 Boston-Providence Turnpike
Norwood, MA 02062 (1)

Federal Emergency Management Agency
Attn: Assistant Associate Director for Research
National Preparedness Programs Directorate
Washington, D.C. 20472 (3)

Federal Emergency Management Agency
Attn: David W. Bensen
Office of Research
National Preparedness Programs Directorate
Washington, D.C. 20472 (45)

Dr. Francis E. Fendell
R1/1038
TRW
One Space Park
Redondo Beach, CA 90278 (1)

Fire Research Library
National Bureau of Standards
Building 224, Room A-246
Washington, D.C. 20234 (1)

Mr. Dick Foster
SRI International
1611 Kent Street
Arlington, VA 22209 (1)

Dr. Robert Fristrom
Johns Hopkins Applied Physics Laboratory
Johns Hopkins Road
Laurel, MD 20810 (1)

Dr. Matthew G. Gibbons
5424 Lawton Avenue
Oakland, CA 94618 (1)

Mr. Edward L. Hill
Research Triangle Institute
P.O. Box 12194
Research Triangle Park,
NC 27709 (1)

Dr. Dennis Holliday
R&D Associates
P.O. Box 9695
Marina del Rey, CA 90291 (1)

Hudson Institute
Attn: Library
Quaker Ridge Road
Croton-on-Hudson, NY 10520 (1)

Mr. Peter S. Hughes
Los Alamos Technical Associates,
Inc.
P.O. Box 410
Los Alamos, NM 87544 (2)

Mr. Robert G. Hutman
Nuclear Test Engineering
Division
Lawrence Livermore National
Laboratory
University of California
P.O. Box 808
Livermore, CA 94550 (1)

Professor A. Murty Kanury
Department of Aerospace and
Mechanical Engineering
University of Notre Dame
Notre Dame, IN 46556 (1)

Mr. Kenneth Kaplan
#30 White Plains Court
San Mateo, CA 94402 (1)

Mr. Samuel Kramer
National Bureau of Standards
Building 225, Room B-124
Washington, D.C. 20234 (1)

Mr. Richard Laurino
Center for Planning and
Research, Inc.
2483 East Bayshore Road,
Suite 104
Palo Alto, CA 94303 (1)

Dr. Anatole Longinow
IIT Research Institute
10 West 35th Street
Chicago, IL 60616 (1)

Los Alamos Scientific Laboratory
Attn: Document Library
Los Alamos, NM 87544 (1)

Mr. Stanley B. Martin
Stan Martin and Associates
860 Vista Drive
Redwood City, CA 94062 (1)

Dr. Clarence R. Mehl
Sandia National Laboratories
Division 7112
P.O. Box 5800
Albuquerque, NM 87185 (1)

Mr. Joseph E. Minor
Texas Technological College
Lubbock, TX 79408 (1)

Mr. H. L. Murphy
P.O. Box 1727
San Mateo, CA 94401 (1)

National Council on Radiation
Protection and Measurements
Attn: Library
7910 Woodmont Avenue
Bethesda, MD 20014 (1)

National Fire Protection Association
Library
Batterymarch Park
Quincy, MA 02269 (1)

Oak Ridge National Laboratory
Attn: Librarian
P.O. Box X
Oak Ridge, TN 37830 (1)

Oak Ridge National Laboratory
Attn: Emergency Technology Division
Librarian
P.O. Box X
Oak Ridge, TN 37830 (1)

Dr. Fred Offensend
SRI International
Menlo Park, CA 94025 (1)

Mr. William Parker
National Bureau of Standards
Building 224, Room A-345
Washington, D.C. 20234 (1)

Professor R. K. Pefley
University of Santa Clara
Santa Clara, CA 95053 (1)

Mr. Laurence Pietrzak
Mission Research Corporation
P.O. Drawer 719
Santa Barbara, CA 93102 (1)

President
International Association of Fire Fighters
1750 New York Avenue, N.W. (3rd Floor)
Washington, D.C. 20006 (1)

Chief Robert G. Purington
Lawrence Livermore National Laboratory
University of California
P.O. Box 808, L-519
Livermore, CA 94550 (1)

The Rand Corporation
Attn: Document Library
1700 Main Street
Santa Monica, CA 90406 (1)

Mr. John Rempel
Center for Planning and Research
2483 East Bayshore Road, Suite 104
Palo Alto, CA 94303 (1)

Dr. John Rockett
National Bureau of Standards
Center for Fire Research
Building 224, Room B-260
Washington, D.C. 20234 (1)

Mr. Harvey G. Ryland
Ryland Research, Inc.
5266 Hollister Avenue, Suite 324
Santa Barbara, CA 93111 (1)

Dr. Donald Sachs
Kaman Sciences Corporation
2001 Jefferson Davis Highway
Arlington, VA 22202 (1)

Mr. Fred Sauer
Physics International Company
2700 Merced Street
San Leandro, CA 94577 (1)

Dr. Don Scheuch
430 Golden Oak Drive
Portola Valley, CA 94025 (1)

Mr. Leo A. Schmidt
Institute for Defense Analyses
Program Analysis Division
1801 N. Beauregard Street
Alexandria, VA 22311 (1)

Mrs. Ruth W. Schnider
Center for Planning and Research, Inc.
2483 East Bayshore Road, Suite 104
Palo Alto, CA 94303 (1)

Southwest Research Institute
Department of Fire Technology
P.O. Drawer 2851D
San Antonio, TX 78284 (1)

Dr. Lewis V. Spencer
National Bureau of Standards
Center for Radiation Research
Building 245, Room C-313
Washington, D.C. 20234 (1)

Mr. Walmer E. Strope
Center for Planning and Research, Inc.
5600 Columbia Pike, Suite 101
Bailey's Crossroads, VA 22041 (1)

Technology & Management Consultants
330 Washington Street
Suite 613
Marina del Rey, CA 90291 (1)

U.S. Army Combined Arms Combat Development Activity
Fort Leavenworth, KA 66027 (1)

U.S. Army Training and Doctrine
Command
Fort Monroe
Hampton, VA 23651 (1)

U.S. Forest Service
Attn: Dr. A. Broido
P.O. Box 245
Berkeley, CA 94710 (1)

Mr. Thomas Watermann
IIT Research Institute
10 West 35th Street
Chicago, IL 60616 (2)

Mr. Carl Wiehle
Defense Intelligence Agency
Attn: WDB-4C2
Washington, D.C. 20301 (1)

Dr. Forman Williams
Department of the Aerospace
and Engineering Sciences
University of California at
San Diego
La Jolla, CA 92037 (1)

Mr. C. Wilton
Scientific Service, Inc.
517 East Bayshore Drive
Redwood City, CA 94060 (2)

International Addresses

Almannavarnir Rikisins
Reykjavik, Iceland (1)

Bundesministerium des Innern
Graurheindorfer Strasse 198
5300 Bonn 1
West Germany (1)

Canadian Defence Research Staff
Attn: Dr. K. N. Ackles
2450 Massachusetts Ave., N.W.
Washington, D.C. 20008 (4)

Civil Defense Administration
Ministry of Interior
Ankara, Turkey (1)

Civil Emergency Planning Directorate
North Atlantic Treaty Organization
1110 NATO, Belgium (1)

Directeur Organisatie
Bescherming Bevoling
Ministry of Interior
Schedeldoekshaven 200
Postbus 20011
2500 The Hague, Netherlands (1)

Directeur de la Protection Civile
Ministere de l'Interieur
36 Rue J. B. Esch
Grand-Duche de Luxembourg (1)

Direction de la Securite Civile
Ministere de l'Interieur
18 Rue Ernest Cognac
92 Levallois (Paris) France (1)

Director
Civilforsvarsstyrelsen
Stockholmsgade 27
2100 Copenhagen 0
Denmark (1)

Forest Fire Research Institute
The Information Center
331 Cooper Street
Ottawa, Ontario KIA 043
Canada (1)

Brigadier I.G.C. Gilmore
Director, Australian Counter
Disaster College
Mount Macedon, Victoria 3441
Australia (1)

The Head of Sivilforsvaret
Sandakerveien 12
Postboks 8136
Oslo dep
Oslo 1, Norway (1)

Home Office
Scientific Advisory Branch
Horseferry House
Dean Ryle Street
London SW1P 2AW
England (1)

Jefe, Seccion de Estudios y
Planification
c/Evaristo San Miguel, 8
Madrid-8
Spain (1)

Ministero dell Interno
Direzione Generale della
Protezione Civile
00100 Rome, Italy (1)

Ministry of Social Services
11 Spartis Street
Athens, Greece (1)

Secretaire d'Administration
Ministere de l'Interieur
Direction Generale de la
Protection Civile
Rue de Louvain, 1
1000 Brussels, Belgium (1)

Dr. Ing. P.G. Seeger
Forschungsstelle fur
Brandschutztechnik
University of Karlsruhe (TH)
75 Karlsruhe 21
Postfach 63380
West Germany (1)

Servico National de
Proteccao Civil
Rua Bela Vista a Lapa, 57
1200 Lisbon, Portugal (1)

Dr. Vilhelm Sjolin
Director of BRANDFORSK
The Swedish Fire Research Board
S-115 87 Stockholm
Sweden (1)

Stato Maggiore Difesa Civile
Centro Studi Difesa Civile
Rome, Italy (1)

ANALYSIS OF THE LARGE URBAN FIRE ENVIRONMENT
Part I. Theory
Unclassified

D. A. Larson and R. D. Small
Pacific-Sierra Research Corporation
12340 Santa Monica Boulevard, Los Angeles, California 90025

PSR Report 1210, July 1982, 34 pp., Contract EMW-C-0747, Work Unit 2564E

The strongly buoyant flow generated in and around a large area fire is analyzed. Jump conditions applicable at the fire periphery are used to effect model problem closure, thus permitting calculations of induced fire winds independent of a far-field analysis. Combustion processes are modeled by a volume heat addition. The induced flow is compressible, with arbitrary changes in temperature and density allowed. In one parameter limit, the model equations can be solved exactly. The resulting solution concisely describes the basic interchanges of energy and momentum as well as the role of pressure gradients in fire-wind generation. In general, the localized analysis provides a framework for detailed studies of the complex physics of fire-generated flows without recourse to extensive numerical computations involving the far field.

The analysis is applied in simulations of the "turning region" environment created by (1) an experimental, multiple-fuel-bed Flambeau fire, and (2) the World War II Hamburg firestorm. Computed results duplicate observed flow patterns and are consistent with reported data.

ANALYSIS OF THE LARGE URBAN FIRE ENVIRONMENT
Part I. Theory
Unclassified

D. A. Larson and R. D. Small
Pacific-Sierra Research Corporation
12340 Santa Monica Boulevard, Los Angeles, California 90025

PSR Report 1210, July 1982, 34 pp., Contract EMW-C-0747, Work Unit 2564E

The strongly buoyant flow generated in and around a large area fire is analyzed. Jump conditions applicable at the fire periphery are used to effect model problem closure, thus permitting calculations of induced fire winds independent of a far-field analysis. Combustion processes are modeled by a volume heat addition. The induced flow is compressible, with arbitrary changes in temperature and density allowed. In one parameter limit, the model equations can be solved exactly. The resulting solution concisely describes the basic interchanges of energy and momentum as well as the role of pressure gradients in fire-wind generation. In general, the localized analysis provides a framework for detailed studies of the complex physics of fire-generated flows without recourse to extensive numerical computations involving the far field.

The analysis is applied in simulations of the "turning region" environment created by (1) an experimental, multiple-fuel-bed Flambeau fire, and (2) the World War II Hamburg firestorm. Computed results duplicate observed flow patterns and are consistent with reported data.

ANALYSIS OF THE LARGE URBAN FIRE ENVIRONMENT
Part I. Theory
Unclassified

D. A. Larson and R. D. Small
Pacific-Sierra Research Corporation
12340 Santa Monica Boulevard, Los Angeles, California 90025

PSR Report 1210, July 1982, 34 pp., Contract EMW-C-0747, Work Unit 2564E

The strongly buoyant flow generated in and around a large area fire is analyzed. Jump conditions applicable at the fire periphery are used to effect model problem closure, thus permitting calculations of induced fire winds independent of a far-field analysis. Combustion processes are modeled by a volume heat addition. The induced flow is compressible, with arbitrary changes in temperature and density allowed. In one parameter limit, the model equations can be solved exactly. The resulting solution concisely describes the basic interchanges of energy and momentum as well as the role of pressure gradients in fire-wind generation. In general, the localized analysis provides a framework for detailed studies of the complex physics of fire-generated flows without recourse to extensive numerical computations involving the far field.

The analysis is applied in simulations of the "turning region" environment created by (1) an experimental, multiple-fuel-bed Flambeau fire, and (2) the World War II Hamburg firestorm. Computed results duplicate observed flow patterns and are consistent with reported data.

ANALYSIS OF THE LARGE URBAN FIRE ENVIRONMENT
Part I. Theory
Unclassified

D. A. Larson and R. D. Small
Pacific-Sierra Research Corporation
12340 Santa Monica Boulevard, Los Angeles, California 90025

PSR Report 1210, July 1982, 34 pp., Contract EMW-C-0747, Work Unit 2564E

The strongly buoyant flow generated in and around a large area fire is analyzed. Jump conditions applicable at the fire periphery are used to effect model problem closure, thus permitting calculations of induced fire winds independent of a far-field analysis. Combustion processes are modeled by a volume heat addition. The induced flow is compressible, with arbitrary changes in temperature and density allowed. In one parameter limit, the model equations can be solved exactly. The resulting solution concisely describes the basic interchanges of energy and momentum as well as the role of pressure gradients in fire-wind generation. In general, the localized analysis provides a framework for detailed studies of the complex physics of fire-generated flows without recourse to extensive numerical computations involving the far field.

The analysis is applied in simulations of the "turning region" environment created by (1) an experimental, multiple-fuel-bed Flambeau fire, and (2) the World War II Hamburg firestorm. Computed results duplicate observed flow patterns and are consistent with reported data.

PSR Report 1210

ANALYSIS OF THE LARGE URBAN FIRE ENVIRONMENT

Part I. Theory

Summary

By
D. A. Larson
R. D. Small

July 1982

Final Report
Contract EMW-C-0747, Work Unit 2564E

For
Federal Emergency Management Agency
National Preparedness Programs
Washington, D.C. 20472

FEMA Review Notice

This report has been reviewed in the Federal Emergency Management Agency and approved for publication. Approval does not signify that the contents necessarily reflect the views and policies of the Federal Emergency Management Agency.

Approved for Public Release: Distribution Unlimited

PACIFIC-SIERRA RESEARCH CORP.
12340 Santa Monica Blvd. • Los Angeles, CA 90025 • (213) 820-2200

SUMMARY

This report analyzes the velocity, temperature, and pressure distributions of a large area fire. The region of interest is the burning area. The analysis considers the effects of massive heating by combustion; the results presented are applicable to the lower surface layer. Predictions of the basic street-level environment can be made and above-shelter air temperatures can be defined. Coupled with an analysis of debris distributions and residual nuclear radiation (fallout or induced activity) in an attacked city, the velocity and temperature predictions will aid in defining the environment facing rescue forces.

This analysis differs considerably from previous treatments. No attempt is made to extrapolate results valid for a free-convection column. The theory presented directly relates the heat release of combustion and size of the burning area to calculated velocities and thermodynamic properties. The induced fire winds depend on the size of the fire and the combustion rate and are, to leading order, independent of the properties of the convective plume.

The results are restricted to large fires (small fires generate a different balance of forces than those considered here). The induced fire winds increase in intensity with heat release or fire size. Compressibility effects limit the maximum velocities attained; however, a continuous spectrum of fire-wind velocities is predicted, ranging from very low levels (corresponding to the experimental Flambeau fires) to high-velocity winds such as generated by the 1943 Hamburg firestorm.

It is clear that the fire is the forcing agent, and external influences are not needed to produce the devastating velocities encountered in the firestorms of World War II. If the fire persists long, swirl may slightly affect the high-velocity winds predicted here.

Sample calculations are presented for the largest Flambeau fires and for the Hamburg firestorm. The results agree with the documented observations and provide insight into the detailed hydrothermodynamic interactions occurring in a large area fire.

A nuclear weapon explosion can ignite fires over much larger areas than those covered by World War II firestorms. The theory developed in this report has been applied to large fires such as may occur in modern urban areas subject to megaton-yield explosions. Those results are presented in Part II of this report.